Ab initio quantum-mechanical study of the effects of the inclusion of iron on thermoelastic and thermodynamic properties of periclase (MgO)

Scanavino I; Belousov R; Prencipe M. Ab initio quantum-mechanical study of the effects of the inclusion of iron on thermoelastic and thermodynamic properties of periclase (MgO). PHYSICS AND CHEMISTRY OF MINERALS. 39 pp: 649-663.
DOI: 10.1007/s00269-012-0519-7

Ab-initio quantum-mechanical study of the effects of the inclusion of iron on thermoelastic and thermodynamic properties of periclase (MgO)

Ab initio study of the effects of the inclusion of iron on the properties of periclase

Summary

1 Abstract
2 Introduction
3 Computational details
    3.1 Basis set, Hamiltonian and computational parameters
    3.2 Geometry, phonon frequencies and Grüneisen's parameters
    3.3 Thermodynamic properties
    3.4 Equation of state
4 Results and discussion
    4.1 Periclase
    4.2 Periclase (Temperature and zero point effects)
    4.3 Ferropericlase
    4.4 Harmonic approximation at high pressure and high temperature conditions
    4.5 Conclusions
5 Tables and Figures
6 References

Isacco Scanavino
Dipartimento di Scienze della Terra,
Università di Torino, Via Valperga Caluso 35,
10125 Torino, Italy
e-mail: iscanavi@unito.it
phone number: +390116705140
fax number: +390116705128

Drawing tools: Qtiplot 0.9.8.4

Ab-initio quantum-mechanical study of the effects of the inclusion of iron on thermoelastic and thermodynamic properties of periclase (MgO)

Isacco Scanavino, Roman Belousov, and Mauro Prencipe

Scanavino I(✉), Belousov R, Prencipe M
Dipartimento di Scienze della Terra,
Università di Torino, Via Valperga Caluso 35,
10125 Torino, Italy
e-mail: iscanavi@unito.it

Abstract

We calculated the thermodynamic and thermoelastic properties of periclase and ferropericlase, the latter having a stoichiometric composition of $(Fe_{0.03}Mg_{0.97})O$, at pressures and temperatures which are typical of the Earth's lower mantle. The static lattice energies and vibrational frequencies were derived through *ab-initio* calculations carried out at the hybrid HF/DFT level. The thermodynamic properties were calculated by following a standard statistical-thermodynamics approach, within the limit of the quasi-harmonic approximation. A third order Birch-Murnaghan equation of state fit to the static *E(V)* data of periclase yielded K_0 = 163.8 GPa, K' = 4.3 and V_0 = 75.09 Å^3. The fit at 300K and 0.1 MPa on the *P(V)* data yielded K_0 = 160.1 GPa, K' = 4.2 and V_0 = 75.99 Å^3. Such results successfully reproduced the best available experimental and previous computational data. The presence of iron with low spin configuration in the structure had the effects (*i*) to reduce the cell volume, both at the static (74.19 Å^3) and at the ambient conditions (75.14 Å^3); (*ii*) to increase the bulk modulus (respectively 172.2 GPa at the static limit, and 167.4 GPa at 298 K and 0.1 MPa) and (*iii*) to decrease the thermal expansion ($2.79*10^{-5}$ K^{-1} for periclase and $2.60*10^{-5}$ K^{-1} for ferropericlase at 300 K). Since the discussed parameters were also calculated at high pressure and temperature conditions simultaneously, the reliability of the quasi-harmonic approximation was tested by evaluating the shape of the potential energy curve, at conditions which simulate those of the Earth's lower mantle. Such test confirmed the applicability of this approximation over all the P/T range considered.

Keywords Periclase, Ferropericlase, lower mantle, thermoelastic properties, quasi-harmonic approximation, quantum-mechanical calculations

Introduction

The Earth's lower mantle (660 – 2890 km depth) is thought to consist mainly of a mixture of Mg-Fe silicate perovskite $(Mg_xFe_{1-x})SiO_3$, ferropericlase $(Mg_yFe_{1-y})O$, and Ca-rich silicate perovskite ($CaSiO_3$; Irifune 1994; Wood 2000). As the information on this deep and inaccessible region is mostly derived from seismic data, which are directly connected to the thermoelastic properties of these phases, it is essential to determine them in order to improve the understanding on the regime and seismic velocities at the Earth interior. In this study we focused on the ferropericlase, an oxide with the NaCl-type structure (space group *Fm*-3*m*), which is likely to be the most abundant non-silicate oxide in Earth (Katsura and Ito 1989; Irifune et al. 1998) and hence it is a phase of crucial importance for the geophysics of the mantle.
At present, most of the studies on ferropericlase were focused on the determination of the depth of the high-low spin transition of the bivalent iron (Lin et al. 2005; Speziale et al. 2005; Persson et al. 2006; Tsuchiya et al. 2006; Lin et al. 2007; Crowhurst et al. 2008), and on the measure of its thermoelastic and electronic properties at different P/T conditions and different Fe/Mg ratios (Hama and Suito1999; Jacobsen et al. 2002; Korotin et al. 1994; Kung et al. 2002; van Westrenen et al. 2005). The Fe/Mg partition coefficient plays a key role for the understanding of the structure and

dynamic of the lower mantle, as it is the main factor in determining (*i*) its composition and its physical properties (Irifune 1994; Mao et al. 1997; Wood 2000), (*ii*) the interaction between the solid mantle and the molten outer core (Hillgren et al. 1996) and (*iii*) the stability fields of both perovskite and ferropericlase (Fei 1996).
Despite the great number of experimental and computational works concerning the compressibility of periclase and its variation with pressure and temperature (see Garai et al. 2009 for an exhaustive reference list on this phase), the same subjects on ferropericlase were much less studied (Fei 1999; Hama and Suito 1999; Jacobsen et al. 2002; Kung et al. 2002) and only in few works an explicit reference to the two different spin phases (respectively labelled as HS and LS, in the following) was taken into account (Lin et al. 2005; van Westrenen et al. 2005; Persson et al. 2006).
One of the objectives of this work was to obtain a more precise dependence of the compressibility of the ferropericlase as a function of pressure, temperature and iron percentage through the use of a fully *ab-initio* quantum-mechanical approach within the framework of the quasi-harmonic approximation (QHA). This approach has demonstrated its ability to provide useful results concerning the compressibility of crystalline compounds (Anderson 1995; Oganov et al. 2002; Ottonello et al. 2010; Ungureanu et al. 2010, 2012; Prencipe et al. 2011), but the reliability of the results depends upon the choice of some key computational parameters (see the section below).
For a better understanding of the changes and of the effects on the MgO structure induced by the presence of iron, we chose to analyze a composition with a very low iron concentration: for this reason we studied the stoichiometric composition $(Fe_{0.03}Mg_{0.97})O$, obtained by replacing one atom of Fe for one of Mg in the 2x2x2 supercell of the conventional MgO cubic cell. Such a low percentage of LS iron on ferropericlase (4.22% in weight) is very difficult to be obtained experimentally and this is confirmed by the fact that, among the works of literature, the minimum percentage of Fe in periclase that we found for the LS phase is 17% (Lin et al. 2005). For this composition we calculated the P/T dependence of bulk modulus, thermal expansion and other thermodynamic quantities (entropy, heat capacity). The results were then compared with those obtained for periclase, which were calculated by following an identical computational approach. The chosen pressure and temperature ranges were those typical of the lower mantle. The bivalent iron in the compound was studied mainly in the LS configuration because the high-low spin transition was determined to fall between 55 and 75 GPa (Lin et al. 2007; Speziale et al. 2005), and we were interested in the properties at the higher pressures of the deepest Earth's lower mantle, up to about 140 GPa. Nevertheless the HS phase was also studied, but only as regards the static lattice energy (*i.e.* with no inclusion of zero point and thermal vibrations).
One of the main limitation in the use of the QHA is that at high temperature this approximation results unreliable due to the shape of the potential energy curve that is supposed to become anharmonic (the problem of the intrinsic anharmonicity has been thoroughly addressed in Oganov and Dorogokupets 2004a). However this problem has never been approached for simultaneous high pressure and high temperature conditions. Since in our calculations we have to simulate conditions up to 140 GPa and 4000K simultaneously, a test on the shape of the potential energy surface is necessary in order to check which are the effects of the intrinsic anharmonicity at these conditions.

The structure of the article is as follows: in the next section we discuss and report the choice of the most important computational parameters; the subsequent section is devoted to a comparison of the results obtained for periclase with experimental and computational data derived from literature, followed by a presentation of the results obtained for ferropericlase. Finally, a brief discussion on the applicability bounds of the quasi-harmonic approximation in the light of our data is reported.

Computational details

The ground state wave functions, the corresponding energies at the static limit (E_{st}; no inclusion of zero point and thermal energies; see Prencipe et al. 2011 for the definition of the different terms employed in the following), the optimized geometries and the vibrational frequencies were calculated from first principles, at different cell volumes, by means of the CRYSTAL09 code (Dovesi et al. 2010) which implements the LCAO (Linear combinations of atomic orbitals) Hartree-

Fock and Kohn-Sham Self-Consistent Field (SCF) method for the study of periodic systems (Pisani et al. 1988). More precisely, the multielectronic wave function was constructed as an antisymmetrized product (Slater determinant) of monoelectronic crystalline orbitals (CO), that are linear combinations of functions centered on each atom of the crystal (LCAO). In turn, atomic orbitals (basis set) were expressed as linear combinations of Gaussian-type functions (GTF).
This method requires the specification of some parameters, among which the most important one is the Hamiltonian, which could be *purely* DFT (in both the LDA or GGA versions) or an hybrid HF/DFT one, which include an *exact*, *non-local*, Hartree-Fock contribution to the *electronic exchange* to correct for the approximate nature of the DFT exchange functionals [see Pisani (1996) for a detailled description of this methodology].

Basis set, Hamiltonian and computational parameters

The initial Gaussian LCAO basis set of elements was composed of the ones from three different sources: the Mg basis set was taken from Causà et al. (1986) then improved by the addition of diffuse *sp* and *d* shells so to obtain a 85-11G* contraction; the original O basis set was that of Ottonello et al. (2008) modified by the addition of a *d* shell to obtain a 84-11G* contraction; the basis set of Valerio et al. (1995) was adopted for Fe corresponding to a 86-41G* contraction scheme. Thereafter, a variational reoptimization of the exponents of the most diffuse Gaussian functions of all the three elements was performed. The improved basis set are reported in the Supplementary Materials (Table S1). The Hamiltonian chosen was the WC1LYP one which is based on the relatively new WC (GGA) exchange functional proposed by Wu and Cohen (2006), mixed with 16% of the *exact non-local* Hartree-Fock exchange, and employing the LYP correlation functional (Lee et al. 1988). Although tested on relatively few phases, WC1LYP provides excellent results as geometries, vibrational frequencies and bulk moduli of silicates and carbonates are concerned (Demichelis et al. 2009; Ungureanu et al. 2010; Prencipe et al. 2011, 2012a, 2012b). In comparison to the B3LYP Hamiltonian (Becke 1993), one of the most widely used hybrid Hartree-Fock/Density-Functional Hamiltonian in the study of crystals, the WC1LYP seems to provide better results as geometries are concerned, while providing almost identically accurate vibrational frequencies [see Zicovich-Wilson et al. (2004), Demichelis et al. (2009), De La Pierre et al. (2011), and Prencipe et al. (2011, 2012a) for a comparison between different functionals]. The DFT contributions to the total energy were evaluated numerically by integrating, over the cell volume, a function of the electron density and of its gradient. The chosen integration grid was the XLGRID one (Dovesi et al. 2010) corresponding to the use of 33222 points for the 2x2x2 supercell of MgO having a volume of 561.06 $Å^3$. The thresholds controlling the accuracy of the calculation of Coulomb and exchange integrals were set to 7 (ITOL1 to ITOL4) and 16 (ITOL5; Dovesi et al. 2010). The diagonalization of the Hamiltonian matrix was performed at four independent $\underline{k}$ vectors in the reciprocal space (Monkhorst net; Monkhrost and Pack 1976) by setting to 3 the shrinking factor IS (Dovesi et al. 2010).

Geometry, phonon frequencies, elastic constants and Grüneisen's parameters

The calculations of optimized geometries, of their E_{st} and of the phonon frequencies, for both periclase and low-spin ferropericlase ($Fe_{0.03}Mg_{0.97}O$, where the iron is in the low spin configuration), were made by using the supercell of 32 formula unit (64 atoms; a 2x2x2 cell with respect to the conventional one). Cell parameters and fractional coordinates were optimized by analytical gradient methods, as implemented in CRYSTAL09 (Dovesi et al. 2010). Geometry optimization was considered converged when each component of the gradient (TOLDEG parameter in CRYSTAL09) was smaller than 0.00001 hartree/bohr and displacements (TOLDEX) with respect to the previous step were smaller than 0.00004 bohr.
The choice of the 2x2x2 supercell for periclase was justified by the requirement of a consistent treatment of the two phases at the same level of accuracy, when the vibrational effects were included: this also allowed the inlcusion of the phonon dispersion effects (32 $\underline{k}$ point belonging to the Irreducible First Brillouin Zone - IBZ) in the estimation of the temperature dependence of the

calculated properties.
The optimizations were made at the static equilibrium (*zero static* pressure; V_0 = 600.19 Å^3 [75.02 Å^3 for the conventional cell] for periclase, V_0 = 593.52 Å^3 [74.19 Å^3] for ferropericlase at the WC1LYP level) and at different unit cell volumes (9 volumes falling in the [389.02, 624.00 Å^3] range, corresponding to static pressures in the [-7, 170 GPa] both for periclase and ferropericlase).
The iron of ferropericlase was studied in both the low and high-spin configurations. As the latter one is concerned, the ranges of the 9 volumes used for the fitting, referred to the supercell, were two; precisely, one range was [529.81, 599.93 Å^3] corresponding to static pressures in the [0, 23 GPa] interval, and the other one was [379.53, 589.33 Å^3] corresponding to static pressures in the [0, 180 GPa] interval. To reach the SCF convergence (Pisani et al. 1988), the calculus for the HS phase required a larger Hartree-Fock contribution to the total electronic exchange (35%, to be compared to the 16% of the standard WC1LYP formulation) and a distortion of the supercell with a reduction of the symmetry from cubic (*Fm*-3*m*) to a tetragonal one (*P4/mmm*; a Jahn-Teller distorsion). For the comparison with the high-spin phase, the static energies of the low-spin one and of the periclase were also recalculated with the same Hamiltonian (35% of exchange Hartree-Fock contribution).
The second-order elastic constants were calculated through a fully-automated procedure based on deformation and optimization of the geometry to obtain the 3x3 force matrix (ELASTCON keyword in CRYSTAL09 - Perger et al. 2009; Dovesi et al. 2010).
Normal vibrational modes and their frequencies were calculated for the nine cell volumes ([389, 624 Å^3] range) within the limit of the QHA, by diagonalizing a mass-weighted Hessian matrix, whose elements were the second derivatives of the full potential of the crystal with respect to mass-weighted atomic displacements (Pascale et al. 2004). The energy first derivatives with respect to the atomic positions were calculated analytically (Doll et al. 2001), whereas second derivatives were calculated numerically by setting to 0.001 Å the nuclear displacements with respect to the equilibrium positions. The threshold for the convergence of the total energy, in the SCF cycles, was set to 10^{-10} hartree (TOLDEE parameter in CRYSTAL09; Dovesi et al. 2010).
For each vibrational mode, the mode-γ Grüneisen's parameter (γ - Anderson 1995) was estimated through the analytical derivative of the frequency as a function of volume reconstructed by curve fitting to a quadratic algebraic polynomial. Higher degree polynomials were not suited because of the insufficiently dense point net (9 volumes) used for the fitting.

Thermodynamic properties

Thermoelastic and thermodynamic properties (total pressures, bulk moduli, thermal expansion, entropy and heat capacity) were obtained in the limit of the QHA, through the evaluation of the dependence of the frequencies of the vibrational normal modes by the unit cell volume (mode-γ Grüneisen's parameters). Intrinsic anharmonic effects (Oganov and Dorogokupets 2004a) were not taken into account, though they could play a role in determining frequencies and Grüneisen's parameters of the modes having high amplitudes especially at high temperature. These effects are particularly important for the low-frequency modes as, most likely, the latter are associated with the largest displacement of the atoms from their respective equilibrium positions.
To check the validity of such choice, a study of the shape of the potential energy curve along two vibrational modes of lowest frequency (SCANMODE keyword in CRYSTAL09; Dovesi et al. 2010) was performed. Through this keyword each nucleus was shifted along its normal coordinates, and the static energy was correspondingly evaluated. In this way it was possible to check if the potential energy surface calculated for the analysed modes was close to the harmonic shape. As a further confirmation, for these two vibrational modes we calculated the energy of the 27 first excited states through a variational approach applied to a quartic anharmonic oscillator, by using a program developed by one of us (Prencipe), which is available upon request.
For the two HS and LS phases of the ferropericlase the enthalpy [$H_{st} = E_{st}(V) + P_{st}V$] was calculated in the whole range of volumes.
For a detailed analysis on the derivation of the thermodynamic quantities used (Grüneisen's parameters, pressure components, Helmholtz energy, entropy, heat capacity and thermal expansion), by following our approach, see Prencipe et al. (2011).

Equation of state

The K_0, K', V_0 and a_0 static parameters at the equilibrium were obtained by fitting $E_{st}(V)$ data to a volume integrated third-order Birch-Murnaghan (Birch, 1952) equation of state (EoS; BM3, for short, in the following). The same parameters at IUPAC standard pressure and temperature conditions (SATP - P = 0.1 Mpa T = 298 K) were obtained by fitting the total $P(V, T)$ curve to BM3 EoS. Other equations of state (Murnaghan, Vinet, Natural Strain) were not used as not suitable for our too broad compression range (Angel 2000).
The static bulk modulus of periclase at the equilibrium was also calculated from the elastic constants as

$$K = 1/3\ (c_{11} + c_{12}) \qquad (1)$$

Results and discussion

The first two sections are focused on the comparison between literature data of periclase and our calculated data, whereas the third one contains an analysis of the behaviour of the ferropericlase having the stoichiometric composition $(Fe_{0.0}Mg_{0.97})O$, in comparison with that of periclase.

Periclase (Static calculations)

The static energies for a 2x2x2 supercell were calculated at 9 different volumes, from 624.00 $Å^3$ (78.00 $Å^3$ for the conventional cell) to 389.02 $Å^3$ (48.63 $Å^3$) including the equilibrium volume of 600.07 $Å^3$ (75.01 $Å^3$). The corresponding pressures ranged from -5.9 GPa (cell volume 624.00 $Å^3$) to 169.5 GPa (389.02 $Å^3$). These volumes were chosen so that they cover the range of pressure of the lower mantle (24 – 136 GPa).
In Table 1 the vibrational frequency of the IR-active mode calculated at the Γ point of the IBZ, at the static equilibrium, was compared with the experimental values; the value here obtained (389 cm^{-1}) is in good agreement with the experimental findings.
The resulting EoS parameters for the static fitting are shown in Table 2. The value of the cell volume was influenced by the Hamiltonian employed: concerning the DFT Hamiltonians, it is commonly known that, in ionic systems, LDA underestimates the cell volume and overestimate the bulk modulus, whereas GGA shows the opposite behaviour with an overestimation of the cell volume and an underestimation of the bulk modulus (Alfredsson et al. 2004). Except for Karki et al. (1997), all the DFT works reported in Table 2 are in line with such trends. The comparison, between the works that used purely DFT-GGA functionals and the ones that used hybrid functionals, showed that the former ones (e.g. Oganov and Dorogokupets 2003a; Oganov et al. 2003b) produce a cell volume which is about 2% larger than the latter ones (e.g. this work; Bredow and Gerson 2000). The overestimation of the cell volume by the B3LYP functional (Bredow and Gerson 2000; Wilson and Muscat 2002) with respect to the WC1LYP one was confirmed by our results (Table 2). In light of these considerations, the value of our cell volume (600.72 $Å^3$ for the supercell – 18.77 $Å^3$ for the unit cell) is to be considered in line with other data reported in literature.
As the bulk modulus is concerned, the LDA functional produced an overestimation of such parameter (Wu et al. 2008; Karki et al. 2000), whereas GGA functionals underestimated it (Oganov and Dorogokupets 2003a). The DFT-LDA functional gave larger values with respect to the ones that used hybrid functionals, as it was confirmed by some literature works (e.g. Prencipe and Nestola 2005). Our value of bulk modulus (163.75 GPa) is in line with this trend. For a more detailed discussion about the role of the Hamiltonian on cell volume and on compressibility see Prencipe and Nestola (2005).
The first derivative of the bulk modulus (K' = 4.273) is in a good agreement with all the other values to which it was compared in Table 2. By fixing the value of K' to 4.09 (value obtained by Wu et al. 2008), the bulk modulus increased to 172.94 GPa; such value is quite close to the K_0 of 173.2 GPa obtained by Wu et al. (2008) themselves. This result further confirms the reliability of the

method. The bulk modulus obtained through the elastic constant has a value of 166.82 GPa (Table 2 - this work C).
The reason for the discrepancies among the results reported in Table 2 has to be attributed to several causes among which: (*i*) the different ranges of pressure investigated (e.g. Oganov et al., 2003b); (*ii*) the equation of state used for the $E_{st}(V)$ fit; and (*iii*) the Hamiltonian employed, as discussed before. Despite the range of pressure influenced the value of the parameters from the BM3 fitting less than the other factors, it was nevertheless possible to observe a trend; precisely, by considering only positive static pressures, the higher were the maximum pressures included in the fitting, the lower was the bulk modulus and higher the K'. The inclusion of points at negative static pressures (cell volumes expanded above the value at the static equilibrium) increased the K_0 and reduced the K'. However, all these changes amounted to only a few GPa for the K_0 and to some decimal point for the K'.
In Figure 1 the values of the static pressure as a function of cell volume, compared with the corresponding values of Karki et al. (1997) and Oganov and Dorogokupets (2003a), show small differences in the whole range of volume explored.

Periclase (Temperature and *zero point* effects)

The EoS parameters were also calculated at SATP conditions (Table 3). The values obtained for the cell volume and for the bulk modulus, as compared to the ones obtained from the static calculation, were influenced by the effect of temperature: the increased internal pressure of the crystal (due to the *zero point* and the thermal components; see a thorough discussion on this point in Prencipe et al. 2011) produced a larger cell volume and a decrease of the bulk modulus. This effect was also observed in Karki et al. (2000), in Wu et al. (2008) and in Oganov and Dorogokupets (2003a), where the bulk modulus was reduced from 181.24 to 170.53 GPa. The value of the cell volume we obtained (76.00 $Å^3$) is slightly overestimated in comparison with the values obtained experimentally, but the value of the bulk modulus (160.14 GPa) is close to the average of the experimental data. Increasing the temperature the corrispondence between our bulk modulus and the literature ones (Inbar and Cohen 1995; Oganov and Dorogokupets 2003a; Sinogeikin et al. 2000) remains very good (Figure 2).
As in the case of the fitting fo the static data, the range of pressure of investigation and the EoS applied were the main causes of differences in the results of Table 3: in the same work of Speziale et al. (2001), the bulk modulus changed by 10 GPa depending upon the EoS applied, whereas in the one of Jacobsen et al. (1993) a change of pressure of investigation of 30 GPa brought to a variation of the bulk modulus of 5 GPa. The range of pressure on the BM3 fitting had the same effects we described for the static BM3 fitting (increase of K_0 with the pressure and contemporary decrease of K'), but such effects were minimal, as it was observed for the static case.
The validity of the BM3 as equation of state was tested by constructing the F–f plots (Angel 2000) for static (Figure S1 in Supplementary materials) and thermal conditions (Figure 3). These plots confirmed that our data are correctly described by a BM3 equation of state. Figure 3 also reports the F-f plot from the data of Jacobsen et al. (2008) and Speziale et al. (2001): while the former data were perfectly described by a BM3, the latter data were not. The slope of the straight lines interpolating the points in Figure 3 is consistent with the fact that our estimation of K' is larger than the one obtained by Jacobsen et al. (2008). This was confirmed by the data of Table 3 where all the K' obtained by computational works are, on average, bigger than those from experimental works (like Jacobsen et al. 2008). Moreover, it is to be noted that, at variance with experimental works, all of the K' reported in computational works are larger than 4, the value for which the F-f plot is a horizontal line.
Some thermodynamic and thermoelastic parameters of interest (entropy S, thermal expansion α, constant pressure C_P and constant volume C_V heat capacity) were calculated at SATP conditions (Table 4). The calculations were performed by using a second order (this work I), a third order (this work II) and a quartic order (this work III) polynomial for the fitting of the frequencies as a function of the volume. The values are in an excellent agreement in comparison with both the experimental and computational data from literature. This agreement remained high as the temperature was

increased also over the assumed limit of validity of the QHA (Figure 4), that for periclase at zero pressure is set to 2000 K (2/3 of the melting temperature; Anderson 1995). The value of the thermal expansion shows a slight underestimation (this work I) with respect to the estimations from different works with which it was compared: this underestimation (Figure 5) is otherwise less than $1*10^{-5}$ K^{-1} at 3000 K, and it is comparable with the values obtained by Oganov and Dorogokupets (2003a) using purely DFT functionals. By using higher order polynomials for the $v(T)$ fit (this work II and III in Table 4), these differences are lowered or disappear. Despite the better results, the use of higher order polynomial is not suitable because of our not large set of frequencies points.
The results exposed in the last section demonstrated that our methodology is able to predict with a very good accuray the experimental results. For this reason, even the analogous results obtained for ferropericlase (see next section) can be considered reliable.

Ferropericlase

The $E_{st}(V)$ calculations of the LS phase were performed for a set of volumes, with optimized geometry, ranging from to 624.00 $Å^3$ to 389.02 $Å^3$ (static equilibrium volume at 593.52 $Å^3$), corresponding to static pressures ranging from -7.7 GPa to 170.6 GPa. For the HS phase we used two ranges of volume: one that falls within its range of stability and corresponding to static pressures in the [0, 23 GPa] interval (in turn, corresponding to the [529.81, 599.94 $Å^3$] volume range; static equilibrium volume at 589.33 $Å^3$); the other one, that covers a broader pressure range (from 0 up to 180 GPa), corresponds to the [379.53, 589.33 $Å^3$] interval. The cell employed was the supercell of 32 formula unit (64 atoms) of periclase in which the Mg^{2+} ion with fractionary coordinates (0 0 0) was substituted by the Fe^{2+} ion (having LS or HS configuration). This substitution maintained the same space group of periclase (*Fm-3m*). The correspondent stoichiometric formula is $(Fe_{0.03}Mg_{0.97})O$.
The parameters of the BM3 static fitting are shown in Table 5 (italic character), together with data from literature, and ordered according the percentage of iron. Two different sets of data obtained in our work are reported: one adopts the original WC1LYP functional, the other one employs an increased Hartree-Fock (HF) exchange percentage for a proper SCF convergence in the case of HS ferropericlase (see the *Computational Details* section). For the low-spin phase, such increase of the HF exchange percentage had the *side* effects to reduce the cell volume and to increase the bulk modulus at the equilibrium, thereby confirming a behaviour that was already observed in other studies (Prencipe and Nestola 2005). Therefore the results obtained through the use of the modified WC1LYP Hamiltonian are meanigful, and should accordingly be used, only for the relative comparison of the properties of LS and HS ferropericlase.
About the static V_0, the results obtained by the optimization of the geometries fully confirmed the trend previously observed in literature, with a decrease of the cell volume of the LS ferropericlase (Fei et al. 2007, Persson et al. 2006) and an increase of the HS one (Person et al. 2006, Bonzcar and Graham 1982, Fei et al. 2007, Jacobsen et al. 2002, Matsui et al. 2012, Komabayashi et al. 2010) with respect the one of the periclase (respectively 73.666 $Å^3$ for HS ferropericlase, 72.661 $Å^3$ for LS ferropericlase and 73.438 $Å^3$ for periclase – Table 5). The same parameter, obtained through the BM3, showed a similar trend, but in this case the compression range on which we fitted the data played a significant role: if we consider the same $P(V)$ range for all the three phases ([0 – 180 GPa] for HS ferropericlase and [0 – 170 GPa] for LS ferropericlase and periclase), we obtain V_0 values that reflect the expected ones; if instead we use a compression range for the HS ferropericlase that falls within its range of stability ([0 – 23 GPa], see Figure 6), the V_0 obtained is lower with respect to the one of periclase. However it must be stressed that this is an apparent decrease of the cell volume as a reduction of the compression range in the fitting brings to a reduction of the V_0 and of the K', and simultaneously an increase of the K_0, like that observed also for periclase. Starting from these observations, the result is consistent with those previously obtained. At SATP conditions for the LS phase, due to the vibrational effects, the cell volume was increased (75.15 $Å^3$ – Table 5) and the bulk modulus was reduced to 167.42 GPa (Table 5), whereas the differences with the corresponding parameters of periclase, at the same P/T conditions, were unchanged (-0.85 $Å^3$ for the cell volume and +7.3 GPa for the bulk modulus).

By comparing our K_0 with data from literature, we noticed an increase of this parameter for LS ferropericlase with respect to the one of periclase, which is consistent with the results reported in all of the quoted works of Table 5; a corresponding increase for the HS phase was observed in most but not all the publications (a reduction is reported in Fei et al. 2007, Jacobsen et al. 2002, Reichmann et al. 2008, Speziale et al. 2007).
We want to stress here again that, for a correct comparison between our data and the literature ones, we must consider that, as written above, the modified WC1LYP Hamiltonian we used had the effect to increase the bulk modulus and to reduce the cell volume with respect to the original WC1LYP Hamiltonian. It means that values of K_0 and V_0 obtained with the modified WC1LYP are likely to be respectively overestimated and underestimated by about 5 GPa and 1 $Å^3$, as it appears to be the case for the LS phase. With these corrections the values of the HS ferropericlase approach the others literature data (170.6 GPa and 74.72 $Å^3$).
About the effect of the increase of iron in the structure, starting from Table 5 we can observe that, besides the increase of the cell volume of HS phase, there is no a clear overall trend. As for K_0, the data of Lin et al. (2005) for the LS phase are evidently diverging from the other ones. To check the reliability of this datum, the $P(V)$ points obtained in that work are fitted in the same compression range by us and by Speziale et al. (2007). Both results are very different (118 GPa by us and 190 GPa by Speziale – Table 5). However these data are obtained by a fitting with a BM3 and not with a BM2, as made in the work of Lin et al. (2005), and the error bar is of ±150 GPa according Speziale.
The pressure stability ranges of the LS and HS phases are depicted in Figure 6 where the difference of enthalpies for both phases is shown as a function of the static pressure. This figure confirmed that the phase transition (at the static limit) occurs at about 56 GPa, consistently with what reported by Lin et al. (2005) and Lin et al. (2007).
In order to investigate the trend of the thermodynamic parameters in the range of P/T conditions of the deepest lower mantle, the bulk modulus and the thermal expansion were calculated as a function of the geotherm (Oganov et al. 2004b), as regards the temperature, and as a function of the geobar (pressure rate as a function of the Earth's depth - Oganov et al. 2004b), as regards the pressure (Figure 7 and 8). It is worth noting that, at such high P/T conditions and differently from the ambient ones, the value of the bulk modulus of the LS ferropericlase was lower than that of periclase (Figure 7), a result which is not observed by any other study, whereas the value of the cell volume was always larger (Figure 9). The thermal expansion of LS ferropericlase is lower than the one of periclase (-0.19^{-5} 1/K at SATP conditions - Table 6) and this trend was observed on the whole range of temperature and pressure of the lower mantle (Figure 8). The variation of these parameters also influenced the heat capacity and the entropy, whose values were lowered in comparison with the ones of periclase (Table 6). The behaviour of the analysed parameters, when vibrational effects are taken into account, was ruled by the values of the Grüneisen's parameters, whose average value at the equilibrium volume (1.257) remained positive and did not significantly change from that of periclase (1.122) (see Figure S2 in Supplementary materials).
Like in the case of periclase, the F – f plots of the ferropericlase were constructed (Figure S3 in Supplementary Materials): for both static and thermal conditions, the BM3 EoS correctly described our data.
The results exposed in this section show how a small percentage of iron in the structure of periclase is enough to significantly change its properties. These effects become more important when the P/T conditions are extremely high, like the ones of the Earth's lower mantle.

Harmonic approximation at high pressure and high temperature conditions

For crystalline solids having positive Grüneisen's parameters, like the periclase, the intrinsic anharmonic effects (Oganov and Dorogokupets 2004a) could become appreciable at very high temperatures, like the ones which are typical of the lower mantle (1600 – 4200 K). For this reason the QHA is considered reliable only up to about 2/3 of the melting temperature (2000K for the periclase). Above this temperature limit the large number of low frequency phonons results in vibrations, which undergo large excursions on the potential energy surface and hence might deviate

significantly from the harmonic oscillation. This effect can be contrasted with the one of pressure which, by compressing the volume, increases the frequencies and reduces the amplitude of oscillation. Therefore the effects of intrinsic anharmonicity at high temperatures should be reduced and should become negligible at high pressures [see Stacey and Isaak (2003) for a detailed explanation].
Since the parameters studied in this work were estimated at conditions of high pressure and high temperature simultaneously (up to 140 GPa and 4000 K), beyond the supposed limit of validity of QHA, to control the validity of results the curvature of the potential energy surface was inspected to see if remained harmonic even at conditions that simulate those of the lower mantle. To perform such check, for two different vibrational modes (*F2g* and *F1u* IRREP) with the lowest frequencies (i.e. those with the largest amplitudes at any given temperature), the shape of potential energy curve was studied by the use of the SCANMODE keyword in CRYSTAL09.
The cell volume chosen was the largest which the periclase can assume at the lower mantle (561 $Å^3$ with reference to the supercell) and the nuclear shift imposed was six times the default one used in the calculus of the frequencies (0.006 Å for each branch of the curve of the energy). These choices were made so to increase the probability for the nuclei to move out of the supposedly harmonic region of the potential energy surface.
By fitting the calculated energies as a function of the nuclear displacement with a quartic polynomial function, the coefficients of the quartic term, for both the mode analyzed, were three order of magnitude smaller than the quadratic term. The cubic term for the *F1u* mode was even smaller (four order of magnitude smaller than the quartic term) and for this reason could be excluded and the curve could be considered symmetric. Moreover, recalculating the frequencies including the anharmonic contribution for the 27 first excited states, the values obtained did not significantly differ from the harmonic frequencies previously calculated (difference within 1 cm^{-1}; Table S2 in Supplementary materials).
It is interesting to note that the same test performed for P/T conditions different from the ones of the Earth's lower mantle, gave quite different results; precisely, at a cell volume of 672.88 $Å^3$ with reference to the supercell, corresponding to T = 3000 K and P = 0.0001 MPa, for the two *F2g* and the *F1u* modes the quartic coefficients of the fitting curves were only one and two order of magnitude smaller than the quadratic terms, respectively; the recalculated frequencies for the 27 first excited states with the anharmonic contribution differed from the harmonic frequencies of up to 5.7 cm^{-1} and 13.8 cm^{-1}, for *F2g* and *F1u* mode respectively (Table S2).
In the light of these results, the real potential energy curve could be approximated to a harmonic one in all the range of temperature and pressure of the lower mantle. At the same time our results confirm the observations of Oganov and Dorogokupets (2004a) on the necessity to include the anharmonic effects at high temperature.
All these assumptions can be made only for crystalline solids with a positive average value of the Grüneisen's parameter, as for negative average value of this parameter, the effect of pressure further reduces the frequencies so that the anharmonic contributions should not be ignored.

Conclusions

In this work, through an *ab-initio* methodology, the static and thermodynamic properties of periclase and of ferropericlase with stoichiometric composition $(Fe_{0.03}Mg_{0.97})O$, were studied. In general the estimated data concerning periclase were in good or excellent agreement with the experimental and computational data reported by other authors. The presence of iron in the structure changed both static and thermodynamic properties: the most evident changes were, at static and ambient conditions, a smaller cell volume, a reduction of compressibility and a lesser thermal expansion coefficient.
A better and more complete description of the behavior of the ferropericlase can be obtained by studying compositions increasingly richer in iron. In fact, this work is only the first of a series having the aim to study the behavior of ferropericlase also at higher iron concentrations.
The study of the shape of the potential energy curve as a function of the nuclear displacement for two normal modes confirmed the hypothesis according to which the quasi-harmonic approximation,

for phases with an average positive value of the Grüneisen parameter, can be applied in all the ranges of pressures and temperatures of the Earth's lower mantle without the necessity of anharmonic corrections. The results confirm that this assumption is valid only for high temperature and high pressure at the same time, which are the conditions that are found in the Earth interior.
As a general remark, the results obtained in this work confirm the ability of the ab initio technology to predict the properties of crystalline materials, even at P/T conditions which are not easily reachable experimentally.

Acknowledgements The author thanks Dr. Ungureanu Crina Georgeta for the helpful discussions and the patience.

Tables and figures

Table 1 – The vibrational frequency of the centre zone of the IBZ measured and calculated at the equilibrium conditions for periclase, considering the unitary cell.

	Frequencies [cm^{-1}]	**Volume [$Å^3$]**	**Methodology**
Jasperse et al. (1966)	408	/	IR spectroscopy
Peckham (1967)	393	74.725	Neutron scattering
Sangster et al. (1970)	393	/	Neutron scattering
Mitchell and Fincham (1993)	386*	75.580*	MD
McCarthy and Harrison (1994)	397*	73.824*	HF
	382*	73.824*	HF + P91
Drummond and Ackland (2002)	413*	74.725*	DFT
This work	389*	75.089*	HF/DFT

The symbol / means that the data is not reported
The abbreviations signify: MD (Molecular Dynamics), HF (Hartree-Fock), P91 (Perdew correlation correction), DFT (Density Functional Theory).
* Computational data.

Table 2 – Results obtained by fitting of the energy on volume data by different EoS. The cell volume V_0 and the cell parameter a_0 are referred to the conventional cell with eight atom of periclase [static conditions].

	Interval of fittng *P(V)* data [GPa]	**EoS**	**K_0 [GPa]**	**K'**	**a_0 [Å]**	**V_0 [Å^3]**	**Hamiltonian**
Karki et al. (1997)	0 – 150	BM4	159.7	4.26	4.251	76.798	LDA + PP
	0 – 150	BM3	159.4	4.28	/	/	LDA + PP
Oganov and Dorogokupets (2003a)	-5 – 150	BM3	151.7	4.212	4.266	77.629	GGA + ECP (large core Mg)
	-5 – 150	BM3	150.839	4.052	4.25	76.595	GGA + ECP (small core Mg)
	-5 – 150	BM3	154.183	4.141	4.237	76.049	GGA + PAW (large core Mg)
	-5 – 150	BM3	150.597	4.103	4.253	76.947	GGA + PAW (small core Mg)
	/	/	172.4*	/	/	/	GGA + PAW
	-5 – 150	BM3	181.24	3.997	4.187	73.425	GGA + PAW
Karki et al. (2000)	0 – 200	BM4	169	4.18	4.197	73.920	LDA + PP
Mehl et al. (1988)	-8 – 95	BM3	172	4.09	4.167	72.355	LDA + LAPW
Oganov et al. (2003b)	-10 – 780	BM3	172.6	4.004	4.24	76.225	GGA + ECP
Wu et al. (2008)	0 – 150	BM4	173.2	4.09	4.162	72.10	LDA + LAPW
	0 – 150	BM4	171.3	4.09	4.196	73.90	LDA + PP
Bredow and Gerson (2000)	-10 – 11	γ	/	/	4.23	75.687	HF/DFT (B3LYP)
Wilson and Muscat (2002)	-12 – 21.5	BM3	156.3(6)	4.0(6)	4.25	76.77	HF/DFT (B3LYP)
Hama and Suito (1999)	0 – 225	Vinet	169.5	4.44	4.191	73.632	/
Persson et al. (2006)	-20 – 200	BM3	153	4.255	77.04	4.100	GGA + PAW
Belmonte (2009)	-10 – 170	BM3	167.01	3.95	4.229	75.612	HF/DFT (B3LYP)
This work A	0 – 170	BM3	163.75	4.273	4.219	75.089	HF/DFT (WC1LYP)
	0 – 170	BM3	172.94	4.09 (fixed)	4.213	74.776	WC1LYP
This work B	0 – 170	BM3	159.02	4.248	4.239	76.176	B3LYP
This work C	/	/	166.82*	/	/	/	WC1LYP

The abbreviations signify: HF/DFT (Hartree-Fock + density functional theory), LDA (local density approximation), GGA (generalized gradient approximation), PP (pseudopotentials), PAW (projector augmented-wave method), ECP (effective core pseudopotentials), LAPW (linearized augmented plane wave).
γ: the cell volume was obtained by the fitting of the data with a forth order polynomial.
* data from elastic constants.
The symbol / means that the data is not reported

Table 3 – Results obtained by fitting of the total pressure on volume data by different EoS. The cell volume V_0 and the cell parameter a_0 are referred to the conventional cell with eight atom of periclase [P = 0.1 MPa, T = 298.15 K].

	Interval of fittng *P(V)* data [GPa]	**EoS**	**K_0 [GPa]**	**K'**	**a_0 [Å]**	**V_0 [Å^3]**	**Methodology [X-ray diffraction]**
Experimental works							
Speziale et al. (2001)	0.8 – 52.2	BM3	160.2 (fixed)	3.99(1)	4.212	74.71(1)	Powder
	0.8 – 52.2	Vinet	160.2 (2)	3.99(1)	4.212	74.71(1)	
	0.8 – 52.2	Poirier	160.2 (6)	4.21(5)	4.212	74.71(1)	
	0.8 – 52.2	BM3	170(1)	3.59(4)	4.208	74.53(2)	
Jacobsen et al. (2008)	0 – 87	BM3	164.6(7)	4.03 (fixed)	4.211	74.69(4)	Single-crystal
	0 – 87	BM3	164.1(9)	4.05(4)	4.211	74.698(7)	
	0 – 118	BM3	159.6(6)	3.74(3)	4.211	74.687(6)	
	0 – 85	BM3	159.5(6)	3.74(3)	4.211	74.697 (7)	
	0 – 118	BM3	160.2 (fixed)	3.709(8)	4.211	74.695(6)	
Jacobsen et al. (2002)	0 – 9	BM3	160	/	4.212	74.698	Single-crystal
Fiquet et al. (1996)	0 – 16	BM3	161(2)	4.5 (fixed)	4.211	74.698	Single-crystal
Fei (1999)	0 – 23	BM3	160(2)	4.15	4.213	74.792	Powder
Dewaele et al. (2000)	0 - 53	BM3	161(1)	3.94(6)	4.212	74.71(1)	Powder
Zha et al. (2000)	0 - 55	BM3	162.5(7)	3.99(3)	/	/	Powder
Kung et al. (2002)	0 – 9	/	162.5	4.13	/	/	Powder
Computational work							
Karki et al. (2000)	0 – 150	BM4	159	4.30	4.222	75.240	LDA + PP
Mehl et al. (1988)	-8 – 95	BM3	164	4.11	4.188	73.455	LDA + LAPW
Oganov and Dorogokupets (2003a)	-5 – 150	BM3	159.94	4.112	4.112	74.712	α
	-5 – 150	BM3 *	170.53	4.036	4.211	74.670	GGA + PAW
Garai (2009)	0 – 148.1	BM3 #	163.59	4.145	4.198	73.975	α
	0 – 148.1	Vinet #	159.42	4.499	4.199	74.028	α
	0 – 148.1	Garai #	165.98	/	4.197	73.909	α
Dorogokupets (2010)	0.8 – 52.2	BM3 *	160.2	3.99	4.212	74.713	β
	0.8 – 52.2	BM3 *	160.64	4.221	4.212	74.713	γ
Wu et al. (2008) [§]	0 – 150	BM4	160	4.23	4.221	75.190	LDA + PP
	0 – 150	BM4	163.2	4.11	4.219	75.110	LDA + PP
	0 – 150	ξ	168.8	4.252	4.202	74.185	LDA + PP
Matsui et al. (2000)	0 – 20	BM4	160.5(2)	4.10(2)	4.211	74.648	MD simulation
Hama and Suito (1999)	0 – 100	Vinet	160.2	4.52	4.212	74.724	/
This work	0 – 170	BM3	160.14	4.234	4.2358	75.999	HF/DFT (WC1LYP)
	0 – 170	BM3	158.19	4.035 (fixed)	4.2380	76.116	HF/DFT (WC1LYP)
	0 – 170	BM3	157.62	4.273 (fixed)	4.2381	76.120	HF/DFT (WC1LYP)

The abbreviations signify: MD (Molecular dynamics), HF/DFT (Hartree-Fock + density functional theory), LDA (local density approximation), GGA (generalized gradient approximation), PP (pseudopotentials), PAW (projector augmented-wave method), LAPW (linearized augmented plane wave).

α: data obtained by treating a large experimental P – V – T dataset.

β: data from Speziale et al. (2001).

γ: data from Wu et al. (2008).

* BM3 with anharmonic contribution.

ξ Coefficients of a fourth-order polynomial fit of temperature dependence of the equation of state parameters.

#: equation of state with thermal dependence.
§ The work does not specify which are the methodological differences between the two results.
The symbol / means that the data is not reported

Table 4 – Comparison of some thermodynamic parameters of interest (C_V, C_P, S, α). The molar quantities are referred to the primitive cell with two atoms [P = 0.1 Mpa , T = 298.15 K].

	Cv [J/(mole*K)]	**Cp [J/(mole*K)]**	**S [J/(mole*K)]**	**α [1/K]**
Experimental works				
Ghose et al. (2006)	36.58	/	26.80	/
Fiquet et al. (1996)	/	/	/	4.90E-05
Dubrovinsky and Saxena (1997)	/	/	/	3.15E-05
Saxena et al. (1993)	36.82	37.35	26.94	3.12E-05
Fei (1995)	/	/	/	3.16E-05
Chopelas (1990)	36.74	/	26.84	3.11E-05
Isaak et al. (1989)	/	37.67	/	3.12E-05
Computational works				
Oganov et al. (2003b)	/	/	26.81	/
Karki et al. (2000)	36.53	37.06	26.65	3.11E-05
This work - I	36.25	36.67	26.22	2.79E-05
This work - II	36.25	36.76	26.27	3.08E-05
This work - III	36.19	37.03	26.14	4.27E-05

Table 5 - Equilibrium values of K_0, K' and V_0 at static (italic character) and at SATP conditions for the high-spin (HS) and the low-spin (LS) ferropericlase ordered on the percentage of iron. In parenthesis the differences respect to the values of the periclase reported in that work. The maximum percentage in iron considered is the 27.5%.

	***P(V)* fitting interval [GPa]**	**% Fe**	**EoS**	**K_0 [GPa]**	**K'**	**V_0 [Å^3]**	**Methodology**
High- spin							
Reichmann et al. (2008)	0 - 9	1.3	#	161.1 (-2)	4.2 (/)	/	Brillouin spectroscopy
This work	*0 -180*	*3*	*BM3*	*175.87 (+0.25)*	*4.243 (+0.005)*	*73.789 (+0.24)*	*HF/DFT (HF 35%)*
This work	*0 - 25*	*3*	*BM3*	*180.82 (+5.21)*	*4.087 (-0.151)*	*73.207 (-0.341)*	*HF/DFT (HF 35%)*
Jackson et al. (2006)	0 - 20	6	#	163 (0)	3.90 (/)	/	Brillouin spectroscopy
Jacobsen et al. (2002)	/	6	/	161° (+1)	/	75.098 (+0.4)	X-ray diffraction
Bonzcar and Graham (1982)	0 – 0.5	8	δ	159.5 (-2.6)	3.66 (+0.55)	75.312 (+0.582)	X-ray diffraction
Jacobsen et al. (2002)	/	15	/	166° (+6)	/	75.633 (+0.935)	X-ray diffraction
Kung et al. (2002)	0 - 10	17	#	165.6 (+3.1)	4.14 (+0.01)	75.848 (/)	X-ray diffraction
Lin et al. (2005)	0 - 55	17	BM3	160.7 (+0.70)	3.280 (-0.72)	/	X-ray diffraction
Lin et al. (2005)	0 - 55	17	Vinet	161.3 (+1.30)	3.25 (-0.75)	/	X-ray diffraction
Matsui et al. (2012)	0 - 53	17	BM3	160 (fixed)	4.08 (/)	75.849 (+1.124)	X-ray diffraction
This work	0 - 53	17	BM3	175.58^{α}	3.11^{α}	76.179^{α}	
Speziale et al. (2007)	0 - 40	17	BM3	157.5 (-2.7)	3.92 (/)	76.10 (/)	X-ray diffraction
Komabayashi et al. (2010)	15 - 72	19	BM2	154.3 (/)	4 (fixed)	76.24 (+1.10)	X-ray diffraction
Speziale et al. (2007)	0 - 40	20	BM3	158 (-2.2)	4.4 (/)	76.030 (/)	X-ray diffraction
This work	0 - 40	20	BM3	154.42^{β}	3.91^{β}	76.140^{β}	
Fei et al. (2007)	0 - 35	20	BM2	158 (-2)	4 (fixed)	76.16 (+1.45)	X-ray diffraction
Jacobsen et al. (2002)	/	24	/	165° (+5)	/	76.333 (+1.635)	X-ray diffraction
Matsui et al. (2012)	0 - 55	25	BM3	160 (fixed)	4.22 (/)	76.372 (+1.647)	X-ray diffraction
Persson et al. (2006)	*-20 - 200*	*25*	*BM3*	*153 (0)*	*4.100 (0)*	*79.120 (+2.08)*	*GGA + PAW*
Jacobsen et al. (2002)	0 – 9.3	27	BM3	158.4 (-1.6)	5.49 (/)	76.336 (+1.638)	X-ray diffraction
This work	0 – 9.3	27	BM3	158.32^{γ}	5.42^{γ}	76.336^{γ}	

Bonzcar and Graham (1982)	0 – 0.5	27.5	δ	167.6 (+5.5)	3.93 (+0.82)	76.187 (+1.457)	X-ray diffraction
Low-spin							
This work	0 - 170	3	BM3	167.42 (+7.28)	4.085 (-0.149)	75.145 (-0.854)	HF/DFT (WC1LYP)
This work	*0 - 170*	*3*	*BM3*	*177.49 (+1.87)*	*4.28 (-0.042)*	*73.261 (-0.288)*	*HF/DFT (HF 35%)*
This work	*0 - 170*	*3*	*BM3*	*172.17 (+8.42)*	*4.10 (-0.173)*	*74.190 (-0.9)*	*HF/DFT (WC1LYP)*
Lin et al. (2005)	55 - 135	17	BM2	250 (+90)	4 (fixed)	/	X-ray diffraction
Lin et al. (2005)	55 - 135	17	Vinet	245 (+85)	4 (fixed)	/	X-ray diffraction
This work	55 - 135	17	BM3	118.22§	4.48§	76.289§	
Speziale et al. (2007)	55 - 135	17	BM3	190§	4.6§	71§	
Speziale et al. (2007)	40 - 134	17	BM3	186 (+25.8)	4.6 (/)	71.39 (/)	X-ray diffraction
Fei et al. (2007)	40 - 95	20	BM2	170 (+10)	4 (fixed)	74.20 (-0.51)	X-ray diffraction
Speziale et al. (2007)	0 - 62	20	BM3	190 (+29.8)	4.6 (/)	71 (/)	X-ray diffraction
Persson et al. (2006)	*-20 - 200*	*25*	*BM3*	*170 (+17)*	*4.100 (0)*	*74.960 (-2.08)*	*GGA + PAW*
Spin not specfied							
Hama and Suito (1999)	*0 - 225*	*20*	*Vinet*	*161.80 (-7.7)*	*4.750 (+0.31)*	*76.192 (+2.56)*	*Thermodynamic model*
Hama and Suito (1999)	0 - 100	20	Vinet	171.80 (+11.6)	4.640 (+0.12)	75.060 (+0.336)	Thermodynamic model
Fei (1999)	/	3	/	160.55* (-0.45)	4.000 (0)	/	/

The symbol / means that the data is not reported
° adiabatic K_0 obtained from elastic constants
* the parameters are calculated by the relation 161 - X_{FeO}
# Finite- strain equation of state taken from Davies and Dziewonski (1975)
δ From elastic constant
α the fitted data are from Matsui et al. (2012)
β the fitted data are from Speziale et al. (2007)
γ the fitted data are from Jacobsen et al. (2002)
§ the fitted data are from Lin et al. (2005)

Table 6 – Comparison of some thermodynamic parameters of interest (C_V, C_P, S, α). The molar quantities are referred to the primitive cell with two atoms [P = 0.1 MPa , T = 298.15 K].

	Cv [J/(mole*K)]	**Cp [J/(mole*K)]**	**S [J/(mole*K)]**	**α [1/K]**
Periclase	36.25	36.67	26.22	2.79E-05
Ferropericlase	35.81	36.20	25.46	2.60E-05

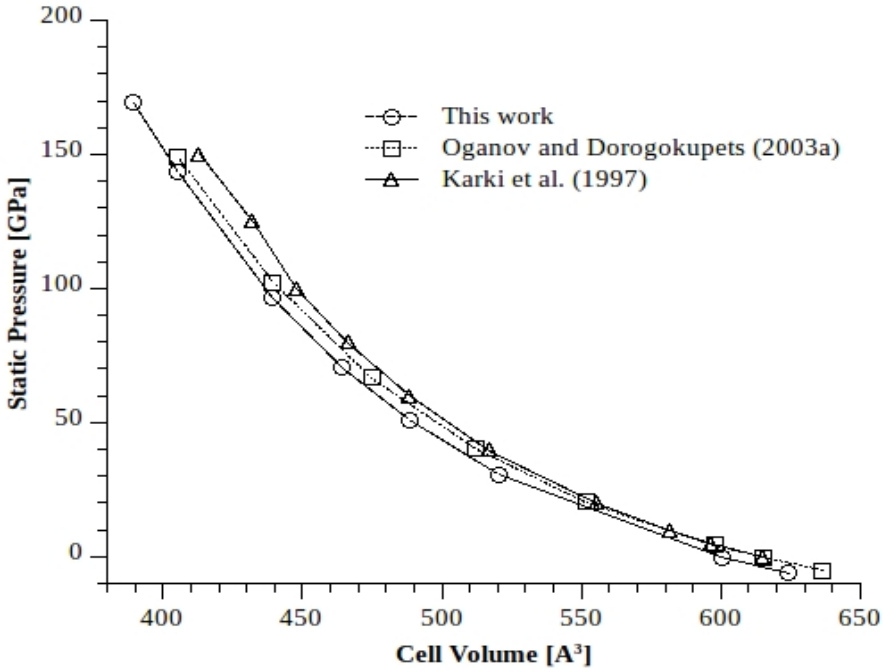

Figure 1 – Static pressure of periclase as a function of the volume of the supercell.

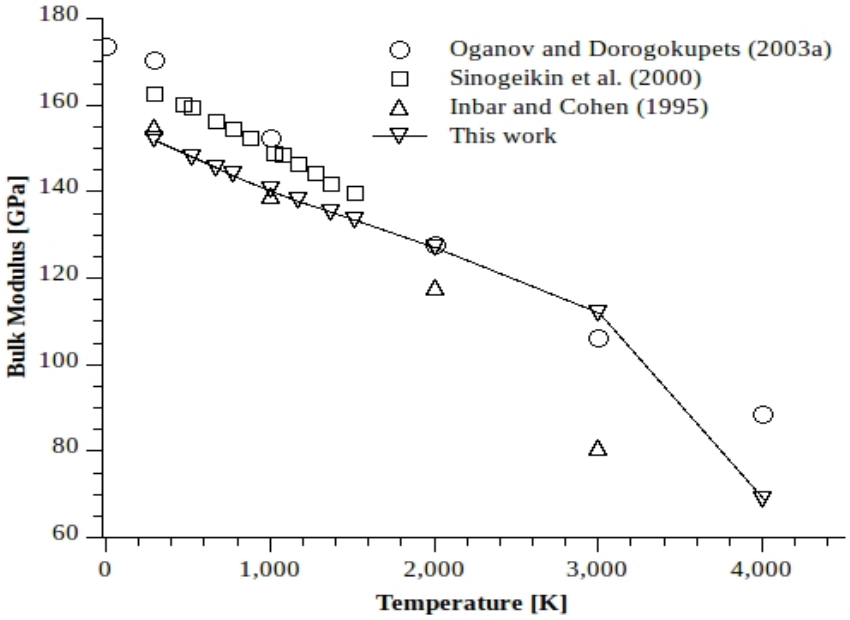

Figure 2 – Bulk modulus of periclase as a function of temperature [P = 0.1 MPa].

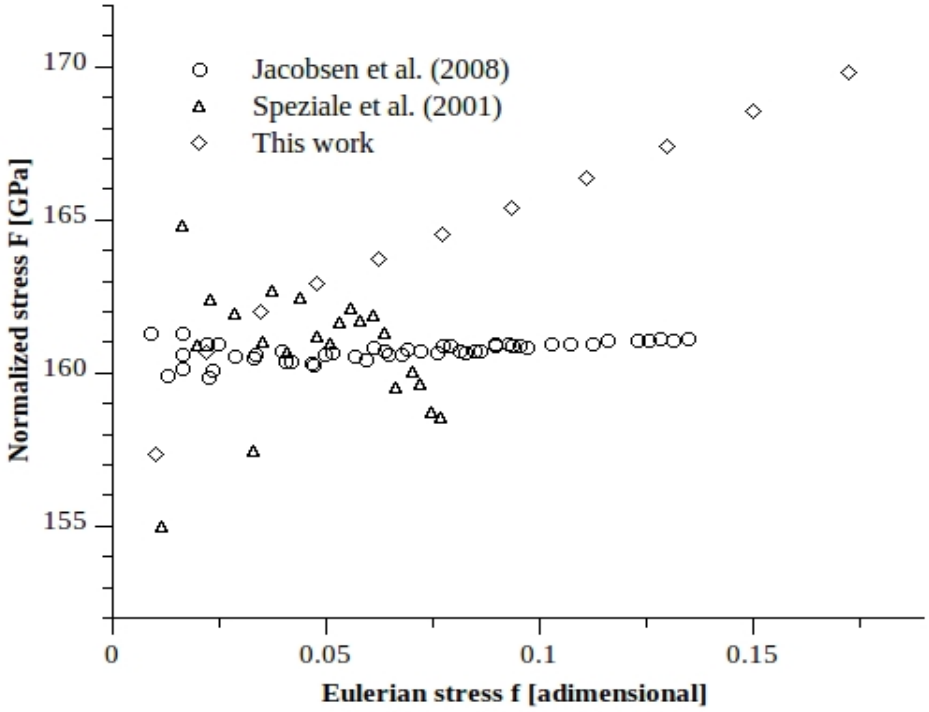

Figure 3 – Normalized stress F as a function of Eulerian strain f for periclase [T = 300 K].

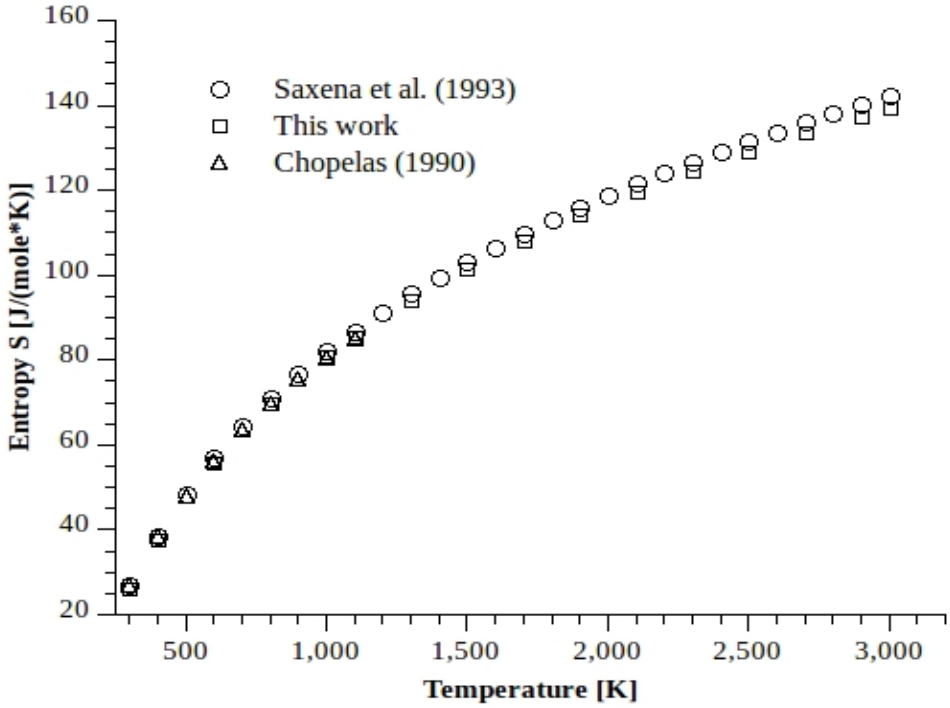

Figure 4 – Entropy of periclase as a function of temperature [P = 0.1 MPa].

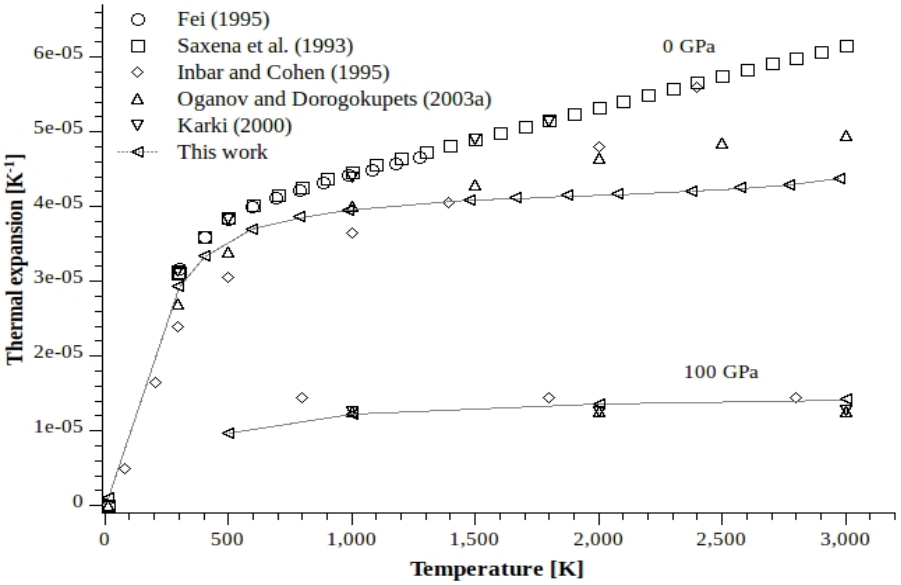

Figure 5 – Thermal expansion coefficient as a function of temperature for different pressures (0.1 MPa and 100 GPa).

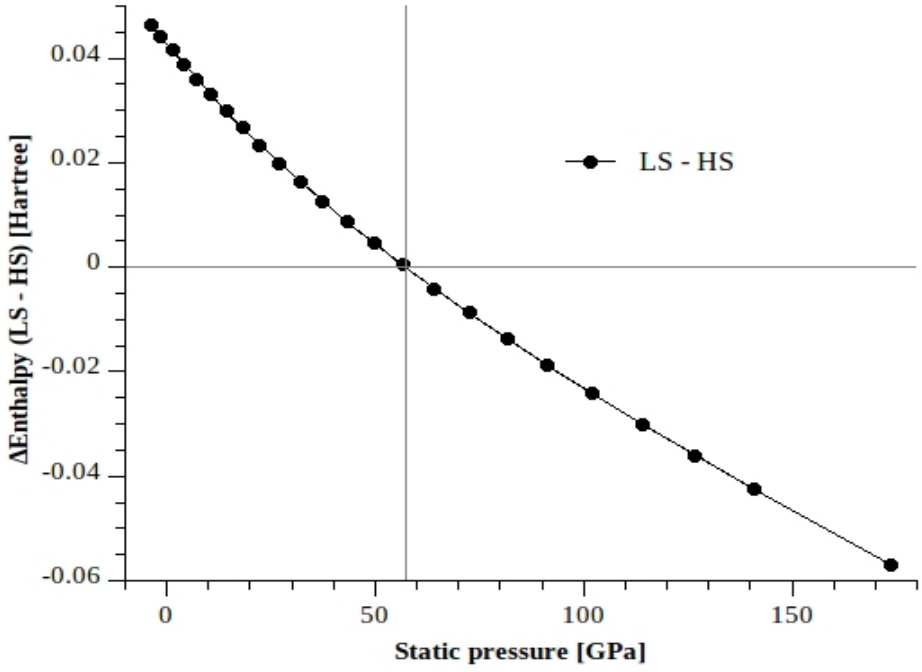

Figure 6 – Entalpy difference between the high-spin and the low-spin phase as a function of the static pressure.

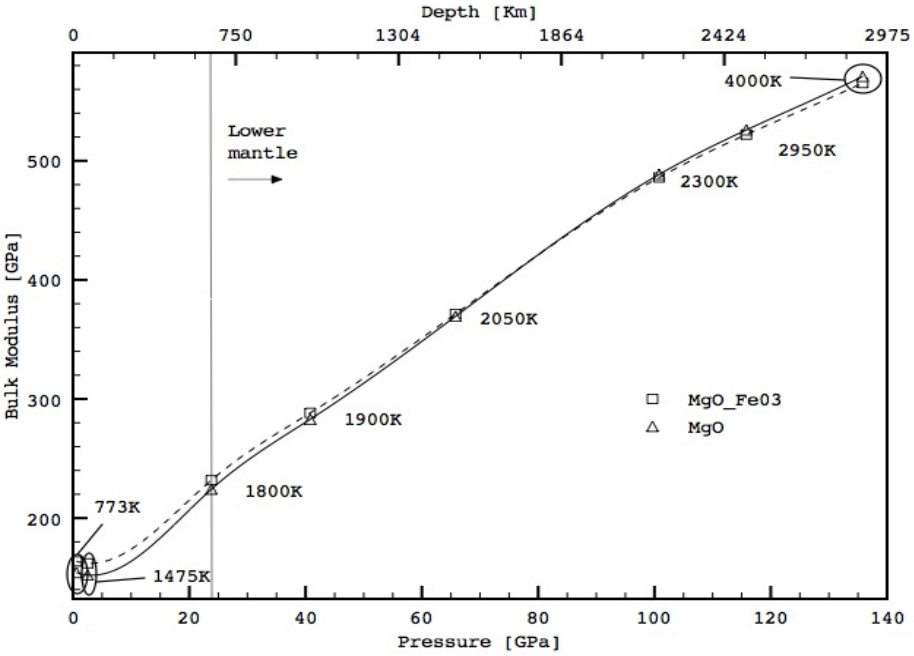

Figure 7 – Bulk modulus as a function of pressure, temperature and depth. The P/T conditions reflect the ones of the Earth's interior according the average value of the geotherm curve and the geobar curve.

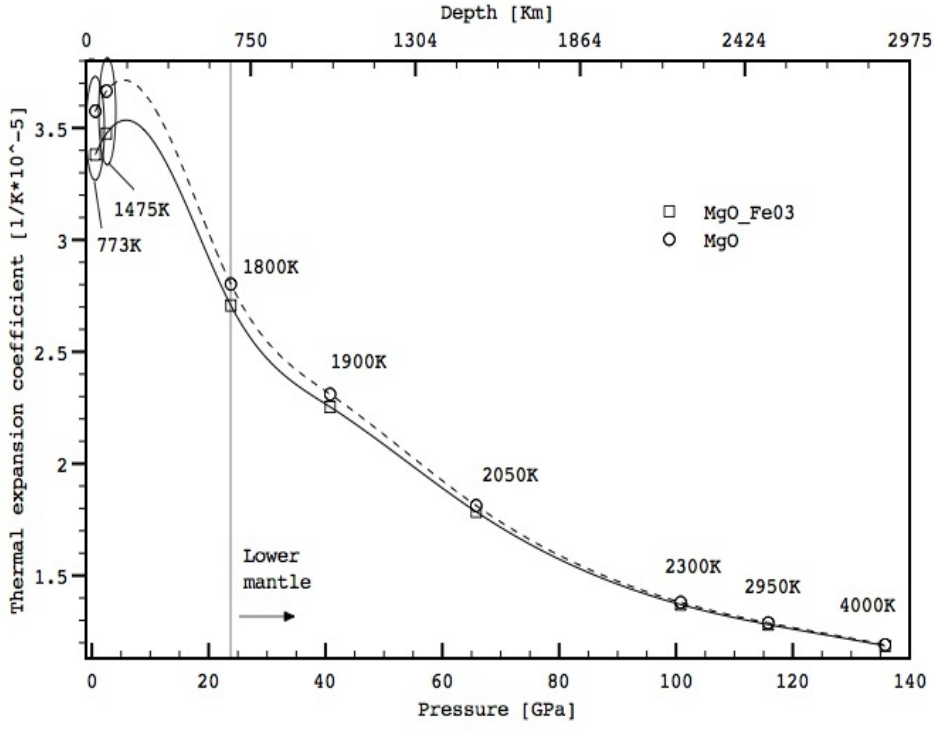

Figure 8 – Thermal expansion coefficient as a function of pressure, temperature and depth. The P/T conditions reflects the ones of the Earth's interior according the average values of the geotherm and the geobara curves.

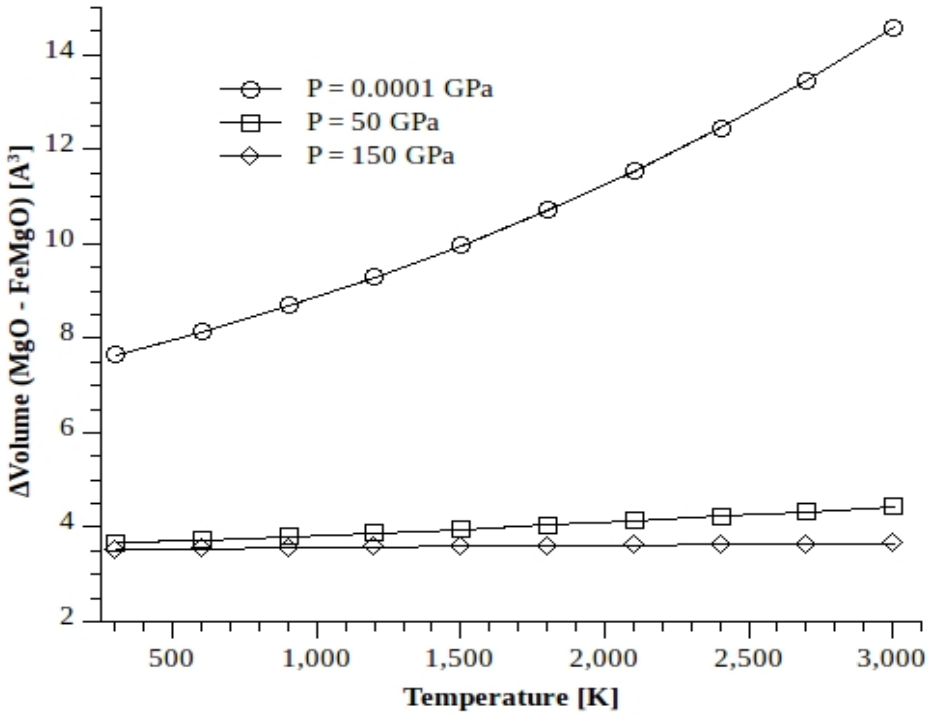

Figure 9 – Differences of volume of the supercells between ferropericlase and periclase as a function of temperature for different pressures.

References

Alfredsson M, Brodholt JP, Wilson PB, Price GD, Cora F, Calleja A, Bruin R, Blanshard LJ, Tyer RP (2005) Structural and magnetic phase transitions in simple oxides using hybrid functionals. Mol Simulat 31: 367 – 377

Anderson OL (1995) Equations of state of solids for geophysics and ceramic science. Oxford University Press, Oxford

Angel RJ (2000) Equations of State. In: Hazen RM, Downs RT: High-temperature and high-pressure crystal chemistry. Rev Mineral Geochem 41: 35 – 39

Becke AD (1993) A new mixing of Hartree-Fock and local density-functional theories. J Chem Phys 98: 5648 - 5652

Belmonte D. Personal communication

Birch F (1952) Elasticity and costitution of the Earth interior. J Geophys Res 57: 227 - 286

Bonzcar LJ and Graham EK (1982) The pressure and temperature dependence of the elastic properties of polycrystal magnesiowustite. Journal of Geophysical Research 87: 1061 - 1078

Bredow T and Gerson AR (2000) Effect of exchange and correlation on bulk properties of MgO, NiO, and CoO. Phys Rev B 61: 5194 - 5201

Causà M, Dovesi R, Pisani C, Roetti C (1986) Electronic structure and stability of different crystal phases of magnesium oxide. Phys Rev B 33: 1308 - 1316

Chopelas A (1990) Thermal expansion, heat capacity, and entropy of MgO at mantle pressures. Phys Chem Minerals 17: 142 - 148

Cremer D (2001) Densuty functional theory: coverage of dynamic and non-dynamic electron correlation effects. Mol Phys 99: 1899 - 1940

Crowhurst JC, Brown JM, Goncharov A, Jacobsen SD (2008) Elasticity of (Mg,Fe)O Through the Spin Transition of Iron in the Lower Mantle. Science 319: 451 - 453

Davies GF and Dziewonski AM (1975) Homogeneity and constitution of the Earth's lower mantle and outer core. Phys Earth Planet Inter 10: 336 - 343

De La Pierre M, Orlando R, Maschio L, Doll K, Ugliengo P, Dovesi R (2011) Performance of six functionals (LDA, PBE, PBESOL, B3LYP, PBE0, and WC1LYP) in the simulation of vibrational and dielectric properties of crystalline compounds. The case of forsterite Mg_2SiO_4. Journal of Computational Chemistry 32: 1775 - 1784

Demichelis R, Civalleri B, Ferrabone M, Dovesi R (2009) On the performance of eleven DFT functionals in the description of the vibrational properties of aluminosilicates. Int J Quant Chem 110: 406 - 415

Dewaele A, Fiquet G, Andrault D, Hausermann D (2000) P-V-T equation of state of periclse from synchrotron radiation measurements. J Geophys Res 105: 2869 - 2877

Doll K, Saunders VR, Harrison NM (2001) Analytical Hartree-Fock gradients for periodic systems. Int J Quantum Chem 82: 1 - 13

Dorogokupets PI (2010) P-V-T equations of state of MgO and thermodynamics. Phys Chem Minerals 37: 677 - 684

Dovesi R, Saunders VR, Roetti C, Orlando R, Zicovich-Wilson CM, Pascale F, Civalleri B, Doll K, Harrison NM, Bush IJ, D'Arco Ph, Llunell M (2010) CRYSTAL09 user's manual. Università di Torino, Torino

Drummond ND, Ackland GJ (2002) Ab initio quasiharmonic equations of state for dynamically stabilized soft-mode materials. Phys Rev B 65: 184104

Dubrovinsky LS and Saxena SK (1997) Thermal Expansion of Periclase (MgO) and Tungsten (W) to Melting Temperatures. Phys Chem Minerals 24: 547 - 550

Fei Y (1995) A Handbook of Physical Constants. AGU Reference Shelf 2: 29 - 44

Fei Y (1996) Crystal chemistry of FeO at high pressure and temperature. In: Dyar MD, McCammon C, Shaefer MW (ed) Mineral Spectroscopy: A Tribute to Roger G. Burns. Special Publication No. 5. The Geochemical Society, Houston, pp.243 - 254

Fei Y (1999) Effects of temperature and composition on the bulk modulus of (Mg,Fe)O. Am Mineral 84: 272 - 276

Fei Y, Zhang L, Corgne A, Watson H, Ricolleau A, Meng Y, Prakapenka V. (2007) Spin transition and equation of state of (Mg,Fe)O solid solutions. Geophysical Research Letters 34:L L17307

Fiquet G, Andrault D, Itie JP, Gillet P, Richet P (1996) X-ray diffraction of periclase in a laser-heated diamone-anvil cell. Phys Earth Planet Inter 95: 1 - 17

Fiquet G, Richet P, Montagnac G (1999) High-temperature thermal expansion of lime, periclase, corundum and spinel, Phys Chem Minerals 27: 103 - 111

Garai J, Chen J, Telekes G (2009) The P-V-T equation of state for periclase. Calphad 33: 737 - 743

Ghose S, Krisch M, Oganov AR, Beraud A, Bosak A, Gulve R, Seelaboyina R, Yang H, Saxena K (2006) Lattice dynamics of MgO at high pressure: theory and experiment. Phys Rev Letters 96: 035507

Grüneisen E (1912) Theorie des festen zustandes einatomizer elemente. Ann Phys (Leipzig) 39: 257 - 306

Hama J and Suito K (1999) Thermoelastic properties of periclase and magnesiowüstite under high pressure and high temperature. Phys Earth Planet Inter 114: 165 - 179

Hillgren VJ, Drake MJ, Rubie DC (1996) High pressure and high temperature metal-silicate partitioning of siderophile elements: The importance of silicate liquid composition. Geochimica et Cosmochimica Acta 60: 2257 - 2263

Inbar I and Cohen RE (1995) High pressure effects on thermal properties of MgO. Geophys Res Lett 22: 1533 - 1536

Irifune T (1994) Absence of an alominous phase in the upper part of the Earth's lower mantle. Nature 370: 131 - 133

Irifune T, Nishiyama N, Kuroda K, Inoue T, Isshiki M, Utsumi W, Funakoshi K, Urakawa S, Uchida T, Katsura T, Ohtaka O (1998) The postspinel phase boundary in Mg_2SiO_4 determined by in situ X-ray diffraction. Science 279: 1698 - 1700

Isaak DG, Anderson OL, Goto T (1989) Measured elastic moduli of single-crystal MgO up to 1800 K. Phys Chem Minerals 16: 704 - 713

Ito E and Takahashi E (1989) Postspinel Transformations in the System Mg_2SiO_4-Fe_2SiO_4 and Some Geophysical Implications. J Geophys Res 94: 15663 - 15670

Jacobsen SD, Reichmann HJ, Spetzler A, Mackwell SJ, Smyth JR, Angel RJ, McCammon CA (2002) Structure and elasticity of single-crystal (Mg,Fe)O and a new method of generating shear waves for gigahertz ultrasonic interferometry. J Geophys Res 107: 2037 - 2051

Jacobsen SD, Holl CM, Adams KA, Fischer RA, Martin ES, Bina CR, Lin JF, Prakapenka VB, Kubo A, Dera P (2008) Compression of single-crystal magnesium oxide to 118 GPa and a ruby pressure gauge for helium pressure media. Am Mineral 93: 1823 - 1828

Jasperse JR, Kahan A, Plendl JN (1966): Temperature dependence of Infrared Dispersion in Ionic Crystals LiF and MgO. Phys Rev 112: 526 - 542

Karki BB, Stixrude L, Clark SJ, Warren MC, Ackland GC, Crain J (1997) Structure and elasticity of MgO at high pressure. Am Mineral 82: 52 – 61

Karli BB (2000) Thermal pressure in MgO and $MgSiO_3$ perovskite at lower mantle conditions. Am Mineral 85: 1447 - 1451

Karki BB, Wentzcovitch RM, De Gironcoli S, Baroni S (2000) High-pressure lattice dynamics and

thermoelasticity of MgO. Phys Rev B 61: 8793 - 8800

Katsura T and Ito E (1989) The System Mg_2SiO_4 - Fe_2SiO_4 at High Pressures and Temperatures: Precise Determination of Stabilities of Olivine, Modified Spinel, and Spinel. J Geophys Res 94: 15663 - 15670

Korotin MA, Postnikov AV, Neumann T, Borstel G, Anisimov VI, Methfessel M (1994) Electronic structure and lattice relaxation related to Fe in MgO. Phys Rev B 49: 6548 - 6552

Kung J, Li B, Weidner DJ, Zhang J, Liebermann RC (2002) Elasticity of $(Mg_{0.83},Fe_{0.17})O$ ferropericlase at high pressure: ultrasonic measurements in conjunction with X-radiation techniques. Earth and Planetary Science Letters 203: 557 - 566

Lee C, Yang W, Parr RG (1988) Development of the Colle-Salvetti correlation-energy formula into a functional of the electron density. Phys Rev B 37: 785 - 789

Lin JF, Struzhkin V, Jacobsen S, Hu M, Chow P, Kung J, Liu H, Mao H, Hemley M (2005) The postspinel phase boundary in Mg_2SiO_4 determined by in situ X-ray diffraction. Nature 436: 377 - 380

Lin JF, Vankó G, Jacobsen SD, Iota V, Struzhkin VV, Prakapenka VB, Kuznetsov A, Yoo CS (2007) Spin Transition Zone in Earth's Lower Mantle. Science 317: 1740 - 1743

McCarthy MI, Harrison NM (1994) Ab initio determination of the bulk properties of MgO. Phys Rev B 49: 8574 - 8582

Mao H, Shen G, Hemley R (1997) Multivariable Dependence of Fe-Mg Partitioning in the Lower Mantle. Science 278: 2098 - 2100

Matsui M, Parker SC, Leslie M (2000) The MD simulation of the equation of state of MgO: Application as a pressure standard at high temperature and high pressure. Am Mineral 85: 312 - 316

Matsui M, Ito E, Yamazaki D, Yoshino T, Guo X, Shan S, Higo Y, Funakoshi KI (2012) Static compression of $(Mg_{0.83}Fe_{0.17})O$ and $(Mg_{0.75}Fe_{0.25})O$ ferropericlase up to 58 GPa at 300, 700, and 1100 K. Am Mineral 97: 176 - 183

Mehl MJ, Cohen RE, Krakauer H (1988) Linearized augmented plane wave electronic structure calculations for MgO and CaO. J Geoph Res 93: 8009 – 8022

Mitchell PJ, Fincham D (1993) Shell model simulation by adiabatic dynamics. J Phys Condens Matter 5: 1031 - 1038

Monkhorst HJ and Pack JD (1976) Special points for Brillouin-zone integration. Phys Rev B 13: 5188 - 5192

Oganov AR, Brodholt JP, Price GD (2002) Ab Initio theory of phase transitions and thermoelasticity of minerals. In: Gramaccioli CM (ed) Energy modelling in minerals. EMU notes in mineralogy, vol 4. Eotvos University Press, Budapest, pp. 83 – 170

Oganov AR and Dorogokupets PI (2003a) All-electron and pseudopotential study of MgO: Equation of state, anharmonicity, and stability. Phys Rev B 67: 224110

Oganov AR, Gillan MJ, Price GD (2003b) Ab initio lattice dynamics and structural stability of

MgO. J Chem Phys 118: 10174 - 10182

Oganov AR and Dorogokupets PI (2004a) Intrinsic anharmonicity in equations of state and thermodynamics of solids. J Phys Condens Matter 16: 1351 - 1360

Oganov AR, Price GD, Scandolo S (2004b) Ab initio theory of planetary materials. Z Kristallogr 220: 531- 548

Ottonello G, Civalleri B, Ganguly J, Vetuschi Zuccolini M, Noel Y (2008) Thermophysical properties of the α - β - γ polymorphs of Mg_2SiO_4: An all-electron ab-initio study. Phys Chem Minerals 36: 87 - 106

Ottonello G, Civalleri B, Ganguly J, Perger WF, Belmonte D, Vetuschi Zuccolini M (2010) Thermo-chemical and thermophysical properties of the high pressure phase Anhydrous B ($Mg_{14}Si_5O_{24}$): an ab initio all-electron investigation. Am Mineral 95: 563 - 573

Pascale F, Zicovich-Wilson CM, Lopez Gejo F, Civalleri B, Orlando R, Dovesi R (2004) The calculation of the vibrational frequencies of crystalline compounds and its implementation in the CRYSTAL code. J Comp Chem 25: 888 - 897

Peckham G (1967) The phonon dispersion relation for magnesium oxide. Proc Phys Soc 90: 657 - 670

Perger WF, Criswell J, Civalleri B, Dovesi R (2009) Ab-initio calculation of elastic constants of crystalline systems with the CRYSTAL code. Comp Phys Comm 180: 1753-1759

Persson K, Bengston A, Ceder G, Morgan D (2006) Ab initio study of the composition dependence of the pressure-induced spin transition in the (Mg_{1-x},Fe_x)O system. Geophysical Research Letters 33: L16306

Pisani C, Dovesi R, Roetti C (1988) Hartree-Fock ab-initio treatment of crystalline systems. Lecture Notes in Chemistry 48. Springer, Berlin Heidelberg New York

Pisani C (1996) Quantum mechanical ab initio calculation of the properties of crystalline materials. Springer Verlag, Berlin.

Prencipe M and Nestola F (2005) Quantum-mechanical modeling of minerals at high pressures. The role of the Hamiltonian in a case study: the beryl ($Al_4Be_6Si_{12}O_{36}$). Phys Chem Minerals 32: 471 - 479

Prencipe M, Scanavino I, Nestola F, Merlini M, Civalleri B, Bruno M, Dovesi R (2011) High-pressure thermoelastic properties of beryl ($Al_4Be_6Si_{12}O_{36}$) from ab initio calculations, and observations about the source of thermal expansion. Phys Chem Minerals 38: 223 - 229

Prencipe M, Mantovani L, Tribaudino M, Bersani D, Lottici PL (2012a) The Raman spectrum of diopside: a comparison between ab initio calculated and experimentally measured frequencies. European Journal of Mineralogy, in press.

Prencipe M (2012b) Simulation of vibrational spectra of crystals by ab initio calculations: an invaluable aid in the assignment and interpretation of the Raman signals. The case of jadeite ($NaAlSi_2O_6$). Journal of Raman Spectroscopy, in press.

Reichmann HJ, Sinogeikin SV, Bass JD. (2008) Single-crystal elastic properties of ($Mg_{0.987}$,$Fe_{0.013}$)O to 9 GPa. American Mineralogists 93: 1306 - 1311

Sangster MJL, Peckham G, Saunderson DH (1970) Lattice dynamics of magnesium oxide. J Phys C: Solid State Phys 3: 1026

Saxena SK, Chatterjee N, Fei Y, Shen G (1993) Thermodynamic Data on Oxides and Silicates. Springer Verlag, Berlin

Sinogeikin SV, Jackson JM, O'Neill B, Palko JW, Bass JD (2000) Compact high-temperature cell for Brillouin scattering measurements. Rev Sci Instrum 71: 201 - 206

Speziale S, Zha C, Duffy TS, Hemley RJ, Mao HK (2001): Quasihydrostatic compression of magnesium oxide to 52 GPa: implications for the pressure–volume–temperature equation of state. J Geophys Res 106: 515 - 528

Speziale S, Milner A, Lee VE, Clark SM, Pasternak MP, Jeanloz R (2005) Iron spin transition in Earth's mantle. Proc Natl Acad Sci USA 102: 17918 - 17922

Speziale S, Lee VE, Clark SM, Lin JF, Pasternak MP, Jeanloz R (2007) Effects of Fe spin transition on the elasticity of (Mg,Fe)O magnesiowüstites and implications for the seismological properties of the Earth's lower mantle. Journal of Geophysical Research 112: B10212

Stacey FD and Isaak DG (2003) Anharmonicity in mineral physics: A physical interpretation. J Geophys Res 108: 2440 - 2446

Tsuchiya T, Wentzcovitch RM, da Silva CRS (2006) Spin Transition in Magnesiowustite in Earth's Lower Mantle. Phys Rev Letters 96: 198501

Ungureanu CG, Cossio R, Prencipe M (2010) Thermodynamic properties of $CaCO_3$ aragonite at high pressure: An ab-initio quantum-mechanical calculation. European Journal of Mineralogy 22: 693 - 701

Ungureanu CG, Cossio R, Prencipe M (2012) Mechanical, Elastic and Thermodynamic properties of calcite ($CaCO_3$) at high pressure: an ab initio quantum-mechanical calculation. Calphad, in press.

Valerio G, Catti M, Dovesi R, Orlando R (1995) Ab initio study of antiferromagnetic rutile-type FeF_2. Phys Rev B 52: 2422 - 2427

van Westrenen W, Li J, Fei Y, Frank MR, Hellwig H, Komabayashi T, Mibe K, Minarik WG, Orman JAV, Watson HC, ichi Funakoshi K, Schmidt MW (2005) Thermoelastic properties of $(Mg_{0.64}Fe_{0.36})O$ ferropericlase based on in situ X-ray diffraction to 26.7 GPa and 2173 K. Phys Earth Planet Inter 151: 163 - 176

Wilson N and Muscat J (2002) The calculation of structural, elastic and phase stability properties of minerals using first principles techniques: a comparison of HF, DFT, and Hybrid functional treatments of exchange and correlation. Mol Simulat 28: 903 - 915

Wood BJ (2000) Phase transformations and partitioning relations in peridotite under lower mantle conditions. Earth Planetary Sci Lett 174: 341 - 354

Wu Z and Cohen RE (2006) More accurate generalized gradient approximation for solids. Phys Rev B 73: 235116

Wu Z, Wentzcovitch RM, Umemoto K, Li N, Hirose K, Zheng J (2008) Pressure-volume-

temperature relations in MgO: An ultrahigh pressure-temperature scale for planetary sciences applications. J Geoph Res 113: B06204

Zha CH, Mao H, Hemley RJ (2000) Elasticity of MgO and a primary pressure scale to 55 GPa. Proc Natl Ac Sci 97: 13494 - 13499

Zicovich-Wilson CM, Pascale F, Roetti C, Saunders VR, Orlando R, Dovesi R (2004) Calculation of the Vibration Frequencies of α-Quartz: The Effect of Hamiltonian and Basis Set. Journal of Computational Chemistry 25: 1873 - 1881